PHYSICAL REVIEW B **96**, 241105(R) (2017)

Giant enhancement of the intrinsic spin Hall conductivity in β-tungsten via substitutional doping

Xuelei Sui,[1,2,3] Chong Wang,[4] Jinwoong Kim,[1] Jianfeng Wang,[2,3] S. H. Rhim,[5] Wenhui Duan,[2,4,*] and Nicholas Kioussis[1,†]

[1]*Department of Physics and Astronomy, California State University Northridge, Northridge, California 91330, USA*

[2]*Department of Physics and State Key Laboratory of Low-Dimensional Quantum Physics, Tsinghua University, Beijing 100084, China*

[3]*Computational Science Research Center, Beijing 100084, China*

[4]*Institute for Advanced Study, Tsinghua University, Beijing 100084, China*

[5]*Department of Physics and Energy Harvest Storage Research Center, University of Ulsan, Ulsan 680-749, Korea*

(Received 12 October 2017; revised manuscript received 23 November 2017; published 19 December 2017)

A key challenge in manipulating the magnetization in heavy-metal/ferromagnetic bilayers via the spin-orbit torque is to identify materials that exhibit an efficient charge-to-spin current conversion. *Ab initio* electronic structure calculations reveal that the intrinsic spin Hall conductivity (SHC) for pristine β-W is about 60% larger than that of α-W. More importantly, we demonstrate that the SHC of β-W can be enhanced via Ta alloying. This is corroborated by spin Berry curvature calculations of $W_{1-x}Ta_x$ ($x \sim 12.5\%$) alloys which show a giant enhancement of the spin Hall angle of up to ≈ -0.5. The underlying mechanism is the synergistic behavior of the SHC and longitudinal conductivity with the Fermi level position. These findings not only pave the way for enhancing the intrinsic spin Hall effect in β-W, but also provide guidelines to exploit substitutional alloying to tailor the spin Hall effect in various materials.

DOI: 10.1103/PhysRevB.96.241105

Current-driven spin-orbit torques (SOTs) in heavy-metal/ferromagnetic heterostructures have drawn increasing attention because they can provide an efficient way of manipulating the magnetization [1–3]. The SOT arises from the transfer of spin angular momentum between the charge current and the local magnetization in the presence of spin-orbit coupling (SOC). The underlying origin of the SOT is still under debate: It may arise from either the bulk spin Hall effect (SHE) [4–7] in the heavy metal or the interfacial SOC [8,9], or both [10,11]. In the SHE, an in-plane charge current density J_c flowing in the heavy metal with strong SOC generates a transverse spin current J_s. The SHE efficiency and the critical current density for magnetization switching is expressed in terms of the spin Hall angle (SHA), $\theta_{\rm SH} = J_s/J_c$ [4,5], which measures the efficiency of the charge current to spin current conversion. It only depends on the material properties and can be experimentally measured via the inverse spin Hall effect [12,13], the spin Seebeck effect [14,15], the Kerr effect [16], or the spin Nernst effect [17].

Relatively large values of $\theta_{\rm SH}$ have been reported in the $5d$ elemental solids of Pt (0.07) [2,18] and the high-resistivity β-Ta (-0.15) [2]. More recently, very thin tungsten films in the highly resistive ($\rho_{\beta\text{-W}} \sim 100$–$300\ \mu\Omega\,$cm) metastable β phase ($A15$ crystal structure) were reported to exhibit a giant spin Hall effect with a $\theta_{\rm SH} \sim -0.3$ to -0.4 [19–21], the largest spin Hall angle among simple element transition metals. In sharp contrast, thicker and/or annealed W films formed in the relatively low-resistivity ($\rho_{\alpha\text{-W}} \leqslant 25\ \mu\Omega\,$cm) α-W phase (bcc crystal structure) exhibit a small (> -0.07) spin Hall angle [19]. These results invite the intriguing question as to the origin in the electronic structure of the dramatically different intrinsic spin Hall conductivities and the spin Hall angles of β- and α-W.

In this Rapid Communication, we compare the intrinsic spin Hall conductivity (SHC) of bulk W in the α (bcc) and β ($A15$) phases using first-principles calculations. The calculations reveal that both phases possess large SHC, where the k-resolved spin Berry curvature elucidates the resonant feature of the spin-orbit splitting of the doubly degenerate bands near the Fermi level. For β-W, the large SHC along with the large resistivity work cooperatively to yield a large SHA. We propose the "acceptor" alloying in β-W can further enhance the SHA from the analysis of the electronic structure. More specifically, Ta substitution locates the Fermi level inside the SOC-induced band gap, rendering the SHC remarkably gigantic, which suggests a way to increase the SHE.

Ab initio electronic structure calculations have been carried out within the framework of the projector augmented-wave formalism [22], as implemented in the Vienna *ab initio* simulation package (VASP) [23–25]. The generalized gradient approximation is used to describe the exchange-correlation functional as parametrized by Perdew-Burke-Ernzerhof [26]. The plane-wave cutoff energy is 500 eV and the first Brillouin zone (BZ) is sampled using a Γ-centered special k-point grid with $24 \times 24 \times 24$ for α-W and $14 \times 14 \times 14$ for β-W, respectively. All structures are fully relaxed with force criteria of 0.001 eV/Å. The SOC of the valence electrons is in turn included using the second-variation method [27] employing the scalar-relativistic eigenfunctions of the valence states. Then, density functional theory (DFT) wave functions were projected to maximally localized Wannier functions using the WANNIER90 package [28–30] and the Kubo formula [31] was employed to calculate the SHC. A dense k mesh of $100 \times 100 \times 100$ and $90 \times 90 \times 90$ on the full BZ for α-W and β-W, respectively, is employed to perform the BZ integration for the intrinsic SHC because of the slow convergence caused by the large contributions of both signs to the spin Berry curvature which occur in very small regions of k space. The longitudinal charge conductivity is calculated using the Boltzmann transport equation [32].

In the clean case (impurity potential $V = 0$), the intrinsic SHC within the Kubo formalism involves an integration of the

*dwh@phys.tsinghua.edu.cn
†nick.kioussis@csun.edu

spin Berry curvature $\Omega_n^z(\boldsymbol{k})$ of the occupied bands over the BZ [7,33],

$$\sigma_{ab}^c = e/\hbar \int_{\mathrm{BZ}} \frac{d\boldsymbol{k}}{(2\pi)^3} \sum_n f_{\boldsymbol{k}n} \Omega_{n,ab}^c(\boldsymbol{k}), \tag{1}$$

where $f_{\boldsymbol{k}n}$ is the Fermi-Dirac distribution function for the nth band at $\boldsymbol{k}$ and the Berry curvature of the nth band is

$$\Omega_{n,ab}^c(\boldsymbol{k}) = -\sum_{n' \neq n} \frac{2\,\mathrm{Im}[\langle \boldsymbol{k}n|\hat{j}_a^c|\boldsymbol{k}n'\rangle\langle \boldsymbol{k}n'|\hat{v}_b|\boldsymbol{k}n\rangle]}{(\varepsilon_{\boldsymbol{k}n} - \varepsilon_{\boldsymbol{k}n'})^2}. \tag{2}$$

Here, $j_a^c = \frac{1}{2}\{s^c, v_a\}$, is the spin current operator, a, b, and c denote the three Cartesian directions x, y, and z, $s^c = (\hbar/2)\beta\Sigma^c$, where β is a 4×4 matrix and Σ^c is the spin operator in the Dirac equation, and $|\boldsymbol{k}n\rangle$ represents the periodic part of the Bloch wave function with energy $\varepsilon_{\boldsymbol{k}n}$. Note that the spin Berry curvature can be large near the band degeneracy. The second-rank SHC tensor σ_{ab}^c describes the spin current (J_s) generated along the ath direction with spin polarization along c due to a charge current (J_e) flowing along the bth direction. Both α- and β-W crystallize in the centrosymmetric cubic lattices: the α phase in bcc with space group $Im\bar{3}m$ (No. 229) while the β phase in the so-called $A15$ structure with space group $Pm\bar{3}n$ (No. 223). Consequently, $\sigma_{xy}^z = -\sigma_{yx}^z = \sigma_{yz}^x = -\sigma_{zy}^x = \sigma_{zx}^y = -\sigma_{xz}^y$ by permutation symmetry.

There has been a longstanding issue of the SHC cancellation in the clean limit (impurity potential $V \to 0$) due to the vertex corrections [34]. We expect that the SHC in the clean limit ($V \to 0$) is given by the intrinsic SHC value ($V = 0$) due to the vanishing vertex corrections under the symmetry of $H(\boldsymbol{k}) = H(-\boldsymbol{k})$ [35,36].

α-W. Figure 1 shows the relativistic band structure and the SHC (σ_{xy}^z) as a function of the Fermi level position $\Delta\mu = \mu - E_F$ (E_F is the Fermi level) for α-W. At $\Delta\mu = 0$, $\sigma_{xy}^z = -785$ $(\hbar/e)$ $(\Omega\,\mathrm{cm})^{-1}$. Its absolute value is smaller than that in Pt [2200 $(\hbar/e)$ $(\Omega\,\mathrm{cm})^{-1}$] [36] but larger than that in Au [400 $(\hbar/e)$ $(\Omega\,\mathrm{cm})^{-1}$] [37]. The magnitude of SHC decreases monotonically as $\Delta\mu$ is raised to about +2.0 eV, where the SHC reverses sign. On the other hand, when $\Delta\mu$ is lowered, the magnitude of the SHC increases considerably, reaching the value of -1058 $(\hbar/e)$ $(\Omega\,\mathrm{cm})^{-1}$ at $E_F = -0.8$ eV (indicated by the green dotted line labeled by 1). The absolute value of σ_{xy}^z reaches its maximum value of 1206 $(\hbar/e)$ $(\Omega\,\mathrm{cm})^{-1}$ at $\Delta\mu = -2.4$ eV, as denoted by the green line (label 2) in Fig. 1. Further lowering of $\Delta\mu$ results in a decrease of SHC, which eventually becomes small for $\Delta\mu < -5.0$ eV, a consequence associated with the vanishing SOC of the $5s$ orbital.

In order to elucidate the origin of the SHC change, we show in Fig. 1(b) the k-resolved spin Berry curvature $\Omega_n^z(\boldsymbol{k})$ of the nth band, where red (blue) denotes a positive (negative) contribution. As shown clearly, double degeneracies which are lifted by spin-orbit coupling result in large SHC. Below -3.0 eV, the dominant contribution arises from regions in the vicinity of the high-symmetry point P with $\Omega_n^z(\boldsymbol{k}) > 0$. As the energy increases, the largest contributions to $\Omega_n^z(\boldsymbol{k})$ arise from the Γ-P symmetry direction with a coexistence of positive and negative values, resulting in $\sigma_{xy}^z = -1206$ $(\hbar/e)$ $(\Omega\,\mathrm{cm})^{-1}$ for $\Delta\mu = -2.4$ eV. As the Fermi level position further rises, the sign of $\Omega_n^z(\boldsymbol{k})$ along the Γ-H direction reverses, leading to another SHC peak at about -0.8 eV, and then its magnitude decreases again.

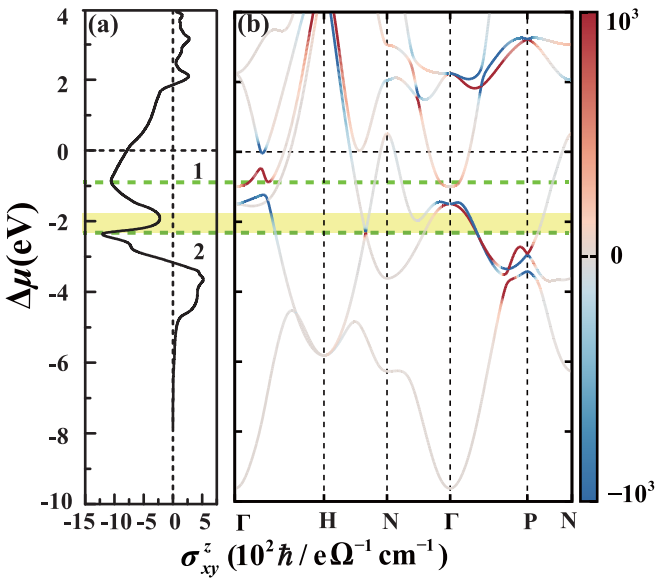

FIG. 1. (a) Spin Hall conductivity as a function of Fermi level position $\Delta\mu$ and (b) relativistic band structure along symmetry directions of α-W. The color denotes the spin Berry curvature $\Omega_n^z(\boldsymbol{k})$ of the nth band for each k point which ranges from negative (blue) to positive (red). The color bar is in arbitrary units. The two green lines through (a) and (b) label the two peaks of SHC. The yellow shaded region denotes the range of $\Delta\mu$ where the SHC displays the largest decrease. The zero energy and the dashed horizontal line is the Fermi level.

β-W. Figure 2(a) shows the band structure and the SHC (σ_{xy}^z) as a function of $\Delta\mu$ for β-W. Interestingly, the SHC is -1255 $(\hbar/e)$ $(\Omega\,\mathrm{cm})^{-1}$ at $\Delta\mu = 0$, which is 60% larger than that of α-W. The variation of SHC with the Fermi level position is more complicated compared to that for the α case due to the more complex band structure. Nonetheless, σ_{xy}^z increases as $\Delta\mu$ is lowered, reaching its maximum value of -1565 $(\hbar/e)$ $(\Omega\,\mathrm{cm})^{-1}$ at $E_F = -0.4$ eV [green horizontal line 1 in Fig. 2(a)] due to the elimination of the large positive contribution of Berry curvature in the energy window from -0.4 to 0 eV. Remarkably, when the SHC reaches its maximum value, the Fermi level lies in the gap along Γ-X, where the band degeneracy is lifted by spin-orbit coupling. Figures 2(b) and 2(c) show the $\mathbf{k}_\parallel$-resolved spin Berry curvature in the two-dimensional (2D) BZ (k_x, k_y) at $k_z = 0$ for the Fermi level position at 0 and -0.4 eV, respectively. As expected, the Berry curvature depends sensitively on $\Delta\mu$ including a sign reversal throughout a large fraction of the BZ, especially along the Γ-X and around the Y-M directions. These changes and the emergence of an overwhelming negative spin Berry curvature in Fig. 2(c) are consistent with the band structure of β-W.

Temperature dependence of SHC. The temperature dependence of the SHC enters through the Fermi-Dirac function $f_{\mathbf{k},n}$ in Eq. (1). We find a weak temperature dependence of the SHC in both the α and β phases (a change of less than 2% from low to high temperature) (see Fig. S1 in the Supplemental Material [38]), in sharp contrast to the strong temperature dependence reported in Pt [36], Pd [37], and the TaAs Weyl

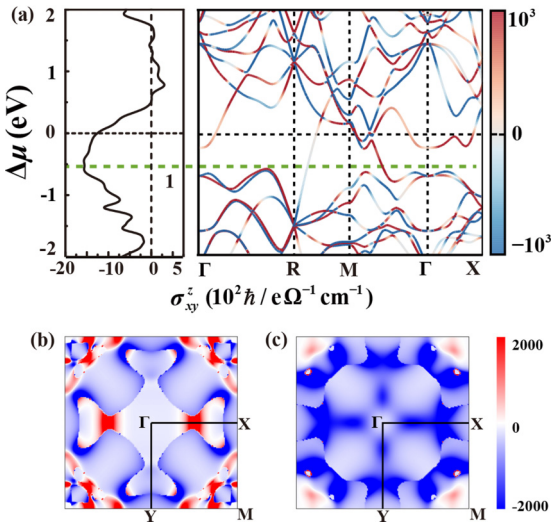

FIG. 2. (a) Spin Hall conductivity as a function of Fermi level position, and relativistic band structure along symmetry directions of β-W. The color denotes the spin Berry curvature $\Omega^z_n(\boldsymbol{k})$ of the nth band for each k point which ranges from negative (blue) to positive (red). The color bar is in arbitrary units. The horizontal green line denotes $\Delta\mu$ at which the SHC is maximum. The $\mathbf{k}_\parallel$-resolved spin Berry curvature in the 2D BZ (k_x,k_y) at $k_z = 0$ for the Fermi level position at (c) 0 eV and (d) -0.4 eV, respectively.

semimetal [39]. The high value of SHC in tungsten, which can be retained even at high temperature, offers a great advantage for room-temperature applications.

Spin Hall angle. The SHA can be expressed as

$$\theta_{\mathrm{SH}} = \frac{e}{\hbar}\frac{\sigma^z_{xy}}{\sigma_{xx}}, \tag{3}$$

where σ_{xx} is the longitudinal charge conductivity, σ^z_{xy} is the transverse spin conductivity (SHC), and the prefactor $\frac{e}{\hbar}$ renders θ_{SH} dimensionless. Obviously, to obtain a large SHA, large SHC as well as low charge conductivity are equally important.

In order to determine the SHA we have also calculated the longitudinal conductivity σ_{xx} using the Boltzmann transport equations within the constant relaxation time approximation [32]. According to the experimental resistivity values of 25 and 300 $\mu\Omega$ cm for α- and β-W [20,40–42], we find that the corresponding room-temperature relaxation times are 5.52 and 1.61 fs, respectively. Assuming that the relaxation time is independent of $\Delta\mu$, we show in Figs. S2(a) and S2(b) (see the Supplemental Material [38]) the variation of the calculated σ_{xx} as a function of $\Delta\mu$ for α- and β-W, respectively. In addition to the larger spin Hall current in β-W, its high resistivity leads to lower Joule heating for the generation of the same amount of spin Hall current. The calculations also reveal that lowering $\Delta\mu \sim -0.2$ eV leads to a much larger increase of σ_{xx} compared to the corresponding increase of SHC [Fig. 1(a)] in α-W, which in turn reduces the SHA to about -0.01. In sharp contrast, lowering $\Delta\mu \sim -0.2$ eV in β-W decreases σ_{xx} while it increases the SHC, resulting in a 47% enhancement of the SHA value (~ -0.47) over its value of -0.32 at $\Delta\mu = 0$ eV, suggesting that the SHA can be enhanced by Fermi level lowering [see Figs. S3(a) and S3(b) in the Supplemental Material [38]]. Table I summarizes values of the SHC at $\Delta\mu = 0$ eV, the maximum $\mathrm{SHC}_{\mathrm{max}}$, the SHA at $\Delta\mu = 0$ eV, and the maximum $\mathrm{SHA}_{\mathrm{max}}$ for the α- and β-W structures, respectively.

TABLE I. Calculated values of the SHC at $\Delta\mu = 0$ eV, the maximum $\mathrm{SHC}_{\mathrm{max}}$, the SHA at $\Delta\mu = 0$ eV, and the maximum $\mathrm{SHA}_{\mathrm{max}}$ for α- and β-W structures, respectively. Experimental values of the SHA are listed in parentheses for comparison. The SHC values are in $(\hbar/e)\ (\Omega\,\mathrm{cm})^{-1}$.

Structure	SHC($\Delta\mu = 0$)	$\mathrm{SHC}_{\mathrm{max}}$	SHA($\Delta\mu = 0$)	$\mathrm{SHA}_{\mathrm{max}}$
α-W	-785	-1206	-0.02 (> -0.07)[a]	-0.03
β-W	-1255	-1565	-0.32 (-0.33, -0.40)[b]	-0.47

[a]Reference [19].
[b]References [19,21].

Alloying β-W with tantalum. In order to corroborate our prediction of the large enhancement of SHC via Ta alloying [see Fig. S3(b) in the Supplemental Material [38]], we have carried out *ab initio* calculations of $W_{1-x}Ta_x$ based on β-W. Since the atomic number of tantalum ($Z_{\mathrm{Ta}} = 73$) is smaller by one unit than that of W ($Z_{\mathrm{W}} = 74$), the substitution of a single W atom by Ta yields one electron missing per unit cell. We considered a Ta atom on four nonequivalent sites in β-W [one for the corner/center site (purple spheres) and three sites on the x, y, and z chains (red, yellow, and green spheres), respectively in Fig. 3(a)]. Figure 3(b) shows the SHC as a function of the Fermi level position $\Delta\mu$ for one Ta substitution on the chain along the x direction. Remarkably, the highest SHC value of -1773 $(\hbar/e)\ (\Omega\,\mathrm{cm})^{-1}$ occurs at $\Delta\mu = 0$ eV, which is a substantial enhancement of 41% over pristine β-W. Moreover, this result is consistent with the SHC at $\Delta\mu \approx -0.2$ eV in pristine β-W [Fig. 2(a)]. Note that the SHC is robust with respect to small variations ($\approx\pm 0.2$ eV) around $\Delta\mu = 0$ eV. Thus, the Ta alloying has a twofold synergistic effect on enhancing the spin Hall angle via increasing the SHC and concurrently decreasing the longitudinal charge conductivity by disorder associated with alloying.

Figure 3(c) shows the $\mathbf{k}_\parallel$-resolved spin Berry curvature in the 2D BZ (k_x,k_y) with $k_z = 0$ for the Fermi level position at $\Delta\mu = 0$ eV. One can see that the $\mathbf{k}_\parallel$-resolved Berry curvature is negative throughout the largest portion of the 2D BZ, which is very similar to that shown in Fig. 2(c) for pristine β-W at $\Delta\mu = -0.4$ eV. This strongly demonstrates that the effect of Ta alloying is equivalent to rigidly lowering the Fermi level position in pristine β-W.

Mechanism of Ta-induced enhancement of SHC. To elucidate the underlying mechanism of the Ta-induced enhancement of SHC, Fig. 3(d) schematically illustrates the doubly degenerate band around the Γ without SOC (gray curves). The SOC splits this double degeneracy with positive (in red) and negative (in blue) spin Berry curvature. If the Fermi level position ($\Delta\mu$) crosses either one of the SOC-split bands, the Berry curvature contributions of both signs tend to cancel each other. This is the case of pristine β-W where $E_F(P)$ crosses the upper band. On the other hand, if the Fermi level position lies in the spin-orbit-coupling-induced gap, the contribution from one sign of Berry curvature is excluded [positive in Fig. 3(d)], resulting in an enhancement of the SHC. This is

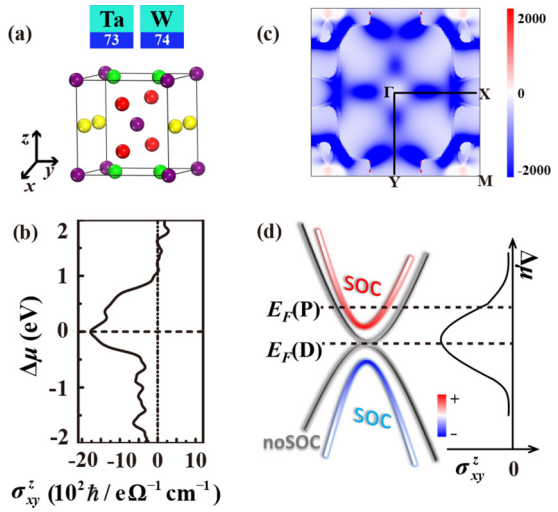

FIG. 3. (a) $A15$ crystal structure of β-W consisting of four nonequivalent sites at the center or corners (purple spheres) and at three atomic chains along the x (yellow spheres), y (green spheres), and z (red spheres) directions, respectively. (b) Spin Hall conductivity σ^z_{xy} vs Fermi level position $\Delta\mu$ for β-W alloyed with tantalum substituting a host atom along the x direction. (c) $\mathbf{k}_\parallel$-resolved spin Berry curvature in the 2D BZ (k_x,k_y) at $k_z = 0$ and for the Fermi level position at 0 eV. (d) Schematic diagram of the band structure around the Γ point without SOC (gray bands) and with SOC (red and blue bands) where the red and blue colors denote bands with positive and negative spin Berry curvature, respectively. $E_F(P)$ and $E_F(D)$ denote the Fermi level positions for pristine β-W and Ta-doped β-W, respectively. We also show schematically the variation of the SHC vs Fermi level position.

the case for Ta-doped β-W where $E_F(D)$ lies in the local gap along the high-symmetry Γ-X direction [see Fig. S3(a) in the Supplemental Material [38]].

Electronic structure calculations are carried out for Ta-alloyed β-W where Ta substitutes one of the W atoms along the y and z chains and at the center sites. We find that the behavior of SHC with Fermi level position is similar to that of Ta occupying a site along the x chain shown in Fig. 3(c) [see Fig. S3(b) in the Supplemental Material [38]], demonstrating that the intrinsic SHC of $W_{1-x}Ta_x$ is remarkably insensitive to variations in the local atomic environment. It should be emphasized that the rigid-band model which shifts the Fermi level inside the spin-orbit-induced local band gap can be used in various systems. Substitution of Ta for W will also cause a large enhancement of the spin Hall effect. Therefore, we provide guidelines to tailor the intrinsic spin Hall effect by a rigid-band model utilizing alloying either with a deficit of or excessive valence electrons.

In summary, using first-principles calculations, we have revealed the physics origin of intrinsic SHC in both tungsten phases. While the β phase exhibits about 60% larger intrinsic spin Hall conductivity than α-W, a much smaller longitudinal conductivity gives a giant spin Hall angle. Moreover, we predict even more gigantic SHC in β-W via Ta alloying $W_{1-x}Ta_x$ ($x \sim 12.5\%$), where a shift of the Fermi level synergistically enhances SHC and reduces the longitudinal conductivity. Finally, we give a general mechanism to improve the intrinsic SHC: Tuning the Fermi level of a system to a spin-orbit-coupling-induced gap can induce a large enhancement of the spin Berry curvature integral. Our results pave an intriguing way towards enhancing the magnitude of SHA and SOT in ferromagnetic/heavy-metal bilayers using Fermi level variations. Our predictions may motivate further experimental studies of the crucial effect of Ta alloying in β-W so as to enhance the SHA and hence optimize the spin-orbit torque efficiency.

We acknowledge the support of the NSF ERC-TANMS Grant No. 1160504, US Army of Defense (DOD), Grant Contract No. W911NF-16-1-0487, Ministry of Science and Technology of China (Grant No. 2016YFA0301001), and the National Natural Science Foundation of China (Grants No. 11674188 and No. 11334006). This work is supported in part by the Beijing Advanced Innovation Center for Future Chip (ICFC). Work at Ulsan is supported by Creative Materials Discovery Program through the National Research Foundation of Korea (2015M3D1A1070465).

[1] I. M. Miron, G. Gaudin, S. Auffret, B. Rodmacq, A. Schuhl, S. Pizzini, J. Vogel, and P. Gambardella, Nat. Mater. **9**, 230 (2010).
[2] L. Liu, C.-F. Pai, Y. Li, H. W. Tseng, D. C. Ralph, and R. A. Buhrman, Science **336**, 555 (2012).
[3] L. Liu, T. Moriyama, D. C. Ralph, and R. A. Buhrman, Phys. Rev. Lett. **106**, 036601 (2011).
[4] M. I. Dyakonov and V. I. Perel, Phys. Lett. A **35**, 459 (1971).
[5] J. E. Hirsch, Phys. Rev. Lett. **83**, 1834 (1999).
[6] T. Jungwirth, J. Wunderlich, and K. Olejník, Nat. Mater. **11**, 382 (2012).
[7] J. Sinova, S. O. Valenzuela, J. Wunderlich, C. H. Back, and T. Jungwirth, Rev. Mod. Phys. **87**, 1213 (2015).
[8] K.-W. Kim, S.-M. Seo, J. Ryu, K.-J. Lee, and H.-W. Lee, Phys. Rev. B **85**, 180404(R) (2012).
[9] H. Kurebayashi, J. Sinova, D. Fang, A. C. Irvine, T. D. Skinner, J. Wunderlich, V. Novák, R. P. Campion, B. L. Gallagher, E. K. Vehstedt, L. P. Zârbo, K. Výborný, A. J. Ferguson, and T. Jungwirth, Nat. Nanotechnol. **9**, 211 (2014).
[10] F. Freimuth, S. Blügel, and Y. Mokrousov, Phys. Rev. B **90**, 174423 (2014).
[11] X. Fan, H. Celik, J. Wu, C. Ni, K.-J. Lee, V. O. Lorenz, and J. Q. Xiao, Nat. Commun. **5**, 3042 (2014).
[12] K. Ando, S. Takahashi, K. Harii, K. Sasage, J. Ieda, S. Maekawa, and E. Saitoh, Phys. Rev. Lett. **101**, 036601 (2008).
[13] O. Mosendz, J. E. Pearson, F. Y. Fradin, G. E. W. Bauer, S. D. Bader, and A. Hoffmann, Phys. Rev. Lett. **104**, 046601 (2010).
[14] K. Uchida, S. Takahashi, K. Harii, J. Ieda, W. Koshibae, K. Ando, S. Maekawa, and E. Saitoh, Nature (London) **445**, 778 (2008).
[15] S. R. Boona, K. Vandaele, I. N. Boona, D. W. McComb, and J. P. Heremans, Nat. Commun. **7**, 13714 (2016).

[16] C. Stamm, C. Murer, M. Berritta, J. Feng, M. Gabureac, P. M. Oppeneer, and P. Gambardella, Phys. Rev. Lett. **119**, 087203 (2017).
[17] S. Meyer, Y.-T. Chen, S. Wimmer, M. Althammer, T. Wimmer, R. Schlitz, S. Geprägs, H. Huebl, D. Ködderitzsch, H. Ebert, G. E. W. Bauer, R. Gross, and S. T. B. Goennenwein, Nat. Mater. **16**, 977 (2017).
[18] A. Azevedo, L. H. Vilela-Leão, R. L. Rodríguez-Suárez, A. F. Lacerda Santos, and S. M. Rezende, Phys. Rev. B **83**, 144402 (2011).
[19] C.-F. Pai, L. Liu, Y. Li, H. W. Tseng, D. C. Ralph, and R. A. Buhrman, Appl. Phys. Lett. **101**, 122404 (2012).
[20] Q. Hao, W. Chen, and G. Xiao, Appl. Phys. Lett. **106**, 182403 (2015).
[21] Q. Hao and G. Xiao, Phys. Rev. Appl. **3**, 034009 (2015).
[22] P. E. Blöchl, Phys. Rev. B **50**, 17953 (1994).
[23] G. Kresse and J. Furthmüller, Phys. Rev. B **54**, 11169 (1996).
[24] G. Kresse and J. Furthmüller, Comput. Mater. Sci. **6**, 15 (1996).
[25] G. Kresse and D. Joubert, Phys. Rev. B **59**, 1758 (1999).
[26] J. P. Perdew, K. Burke, and M. Ernzerhof, Phys. Rev. Lett. **77**, 3865 (1996).
[27] D. D. Koelling and B. N. Harmon, J. Phys. C: Solid State Phys. **10**, 3107 (1977).
[28] G. H. Wannier, Phys. Rev. **52**, 191 (1937).
[29] A. A. Mostofi, J. R. Yates, Y.-S. Lee, I. Souza, D. Vanderbilt, and N. Marzari, Comput. Phys. Commun. **178**, 685 (2008).
[30] I. Souza, N. Marzari, and D. Vanderbilt, Phys. Rev. B **65**, 035109 (2001).
[31] M. Marder, *Condensed Matter Physics* (Wiley, New York, 2000).
[32] G. Pizzi, D. Volja, B. Kozinsky, M. Fornari, and N. Marzari, Comput. Phys. Commun. **185**, 2311 (2014).
[33] G. Y. Guo, Y. Yao, and Q. Niu, Phys. Rev. Lett. **94**, 226601 (2005).
[34] J.-I. Inoue, G. E. W. Bauer, and L. W. Molenkamp, Phys. Rev. B **70**, 041303(R) (2004).
[35] S. Murakami, Phys. Rev. B **69**, 241202(R) (2004).
[36] G. Y. Guo, S. Murakami, T.-W. Chen, and N. Nagaosa, Phys. Rev. Lett. **100**, 096401 (2008).
[37] G. Y. Guo, J. Appl. Phys. **105**, 07C701 (2009).
[38] See Supplemental Material at http://link.aps.org/supplemental/10.1103/PhysRevB.96.241105 for detailed calculation results of spin Hall conductivity versus temperature, charge conductivity, spin Hall angle, and band structures.
[39] Y. Sun, Y. Zhang, C. Felser, and B. Yan, Phys. Rev. Lett. **117**, 146403 (2016).
[40] D. Choi, B. Wang, S. Chung, X. Liu, A. Darbal, A. Wise, N. T. Nuhfer, K. Barmak, A. P. Warren, K. R. Coffey, and M. F. Toney, J. Vac. Sci. Technol. A **29**, 051512 (2011).
[41] S. M. Rossnagel, I. C. Noyan, and C. Cabral, Jr., J. Vac. Sci. Technol. B **20**, 5 (2002).
[42] P. D. Desai, T. K. Chu, H. M. James, and C. Y. Ho, J. Phys. Chem. Ref. Data **13**, 1069 (1984).